Check for updates

Adding the latency period to a muscle contraction model coupled to a membrane action potential model

Nadia Roberta Chaves Kappaun[1,2],
Ana Beatriz Nogueira Rubião Graça[1],
Gabriel Benazzi Lavinas Gonçalves[1], Rodrigo Weber dos Santos[1],
Sara Del Vecchio[3] and Flávia Souza Bastos[1]*

[1]Graduate Program in Computational Modeling, Federal University of Juiz de Fora, Juiz de Fora, Brazil,
[2]National Cancer Institute, Rio de Janeiro, Brazil, [3]Federal Institute of Education, Science and Technology
of the Southeast of Minas Gerais, Juiz de Fora, Brazil

Introduction: Skeletal muscle is responsible for multiple functions for maintaining energy homeostasis and daily activities. Muscle contraction is activated by nerve signals, causing calcium release and interaction with myofibrils. It is important to understand muscle behavior and its impact on medical conditions, like in the presence of some diseases and their treatment, such as cancer, which can affect muscle architecture, leading to deficits in its function. For instance, it is known that radiotherapy and chemotherapy also have effects on healthy tissues, leading to a reduction in the rate of force development and the atrophy of muscle fibers. The main aim is to reproduce the behavior of muscle contraction using a coupled model of force generation and the action potential of the cell membrane, inserting the latency period observed between action potential and force generation in the motor unit.

Methods: Mathematical models for calcium dynamics and muscle contraction are described, incorporating the role of calcium ions and rates of reaction. An action potential initiates muscle contraction, as described by the Hodgkin–Huxley model. The numerical method used to solve the equations is the forward Euler method.

Results and Discussion: The results show dynamic calcium release and force generation, aligning with previous research results, and the time interval between membrane excitation and force generation was accomplished. Future work should suggest simulating more motor units at the actual scale for the possibility of a comparison with real data collected from both healthy individuals and those who have undergone cancer treatment.

KEYWORDS

skeletal muscle model, muscle contraction, latency period, calcium dynamics, action potential model, finite-difference method

1 Introduction

Skeletal muscle is an efficient and adaptable tissue responsible for multiple functions for maintaining energy homeostasis and daily activities [1]. It is composed of blood vessels, connective tissues, and muscle cells known as muscle fibers. A muscle fiber is a long and slender cell whose primary component is the myofibril. Myofibrils play a central role in initiating muscle cell contractions due to the presence of two vital filament types: actin and myosin [2].

Muscle fibers produce force through electrical activation by the nervous system, allowing for muscle contraction and, consequently, motion (Peterson and Bronzino [3]). The interaction between a nerve and a muscle fiber is known as a synapse, and the entire process is initiated by the arrival of an action potential. A motor unit (MU) comprises all the muscle cells controlled by a single nerve fiber. The nerves responsible for controlling muscles are known as motor neurons [2].

Motor units are controlled through synchronous recruitment by the central nervous system. This type of recruitment, as shown in Figure 1, recruits one unit at a time to maintain constant tension and, if necessary, recruits different motor units simultaneously to generate greater tension in the muscle [4]. Farina et al. [5] stated that recruitment begins with the smallest muscle fibers, which typically exhibit the lowest conduction velocity. The controlled activation of motor unit populations accomplishes movement, as described in [6], which was based on the understanding of motor unit physiology through computational and experimental studies. However, muscles do not develop tension immediately; instead, there is a brief period known as the latency period before tension is generated [2].

The contractile system of skeletal muscles is regulated by ions Ca^{2+}, which are stored in the sarcoplasmic reticulum (SR). It was stated in [2] that the release of ions Ca^{2+} into the cytoplasm of muscle cells is triggered by the arrival of an action potential at the motor end plate, followed by neurotransmitter release and uptake by the muscle cells. When Ca^{2+} is removed from the cytoplasm, the contraction process ceases, and the muscle returns to its initial length. The net effect of a single action potential results in a transient contraction of the motor unit, commonly referred to as a *twitch*.
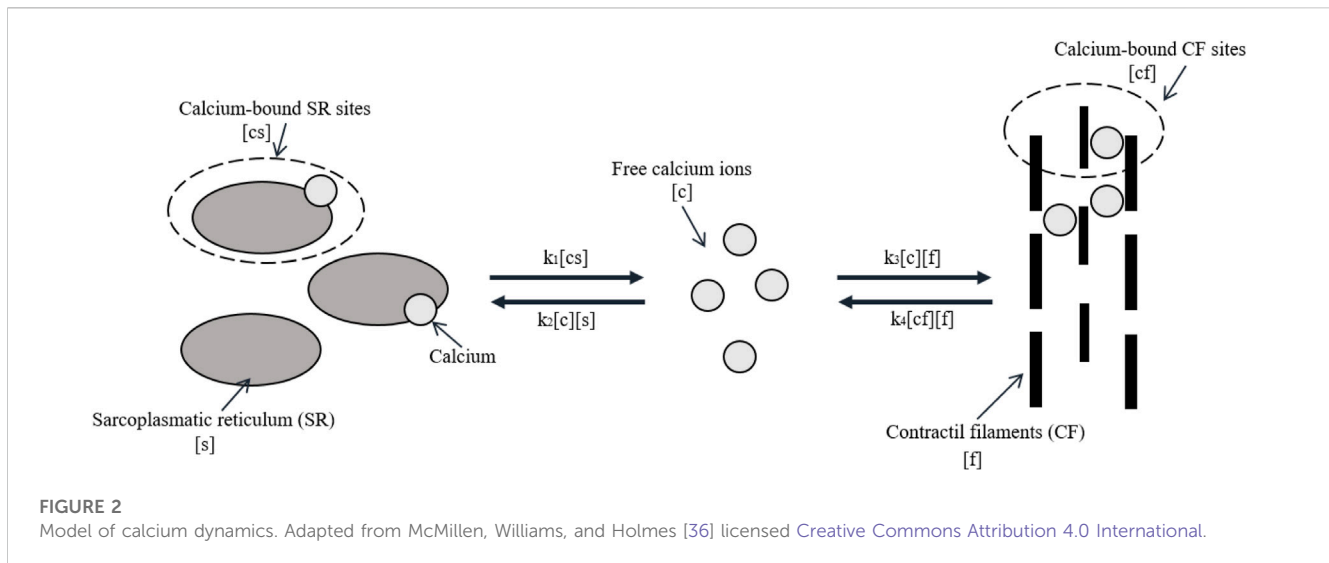
Studying skeletal muscle and its physiological functioning can be important for understanding its behavior in medical conditions, such as muscle fatigue [8,9], bone diseases [10,11], muscular damage [12], dystrophies [13], and diseases of treatment sequelae [14–19]. Commonly used cancer treatments, including chemotherapy [20–22] and radiation therapy [23], affect skeletal muscle, inducing a decrease in the rate of force development and loss in muscle fibers, which leads to a change in muscle function and promotion of its inflammation [17]. It was stated in [18] and [19]that cancer survivors experience several treatment-related symptoms, muscular weakness, and reduced mobility, thereby compromising their quality of life. Furthermore, after pelvic radiotherapy, the exposure of the anal canal and nerves of the sacral plexus to radiation may be associated with the deterioration of sphincter function [24], and changes are observed in the composition of the

FIGURE 1
Tension developed in each MU, resulting in a constant tension in the muscle.
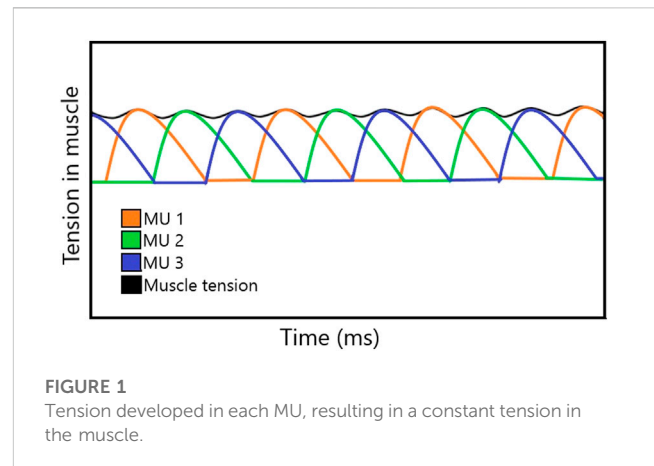
pelvic floor muscle structure, which was maintained even after 4 years of treatment for prostate or colorectal cancer [25]. In addition, functional modifications in the pelvic floor have been reported, such as reduced pressures at rest and during maximum contraction after radiotherapy, for up to 1 year after treatment [26]. It was suggested in [23] that ionizing irradiation leads to a reduction in the perimeter and contractility of muscle fibers as well as a lower amount of skin fiber renewal. Late effects of radiotherapy include gastrointestinal, urological, female reproductive tract, skeletal, and vascular toxicity, secondary malignancies, and quality-of-life issues [27–29].

Recent studies focused on the association between skeletal muscle quality and the prognosis of patients with gynecological cancer [14–16,30]. In [15], it was shown that maintaining muscle mass can prolong survival in cancer patients, and the work in [16] related that visceral obesity before radiotherapy and chemotherapy has a protective effect on the prognosis of patients with stage IVB cervical cancer, while a low muscle index and low visceral-to-subcutaneous adipose tissue area ratio are associated with worse prognosis. Research studies also identified a low pretreatment skeletal muscle index as a prognostic factor for overall survival in patients diagnosed with cervical or ovarian cancer [14,31]. On the other hand, in [30], data from the skeletal muscle area were reviewed to identify skeletal muscle mass loss (sarcopenia) in patients with cervical, endometrial, and ovarian cancers, appointing that the limited literature data seem to suggest that baseline muscle indexes have an uncertain prognostic pertinence, whereas their changes during treatment often correspond with chances of patient survival. Although a novel sarcopenia measure combining quantity and quality of muscle is important to spread the basis to explain the relationship between sarcopenia and solid tumor aftereffects considering high-risk patients [31], there is a lack of studies that analyze muscle changes during cancer treatments, which might be justified by the discrepancy in measurement methods of muscle depletion across research studies [17].

The overall electrical activity of skeletal muscles can be measured by electromyography (EMG). However, EMG signals are difficult to interpret since they are controlled by the nervous system and are dependent on the anatomical and physiological properties of muscles [32]. Additionally, for breast cancer

FIGURE 2
Model of calcium dynamics. Adapted from McMillen, Williams, and Holmes [36] licensed Creative Commons Attribution 4.0 International.

patients, surgery and radiation therapies impact shoulder muscle health throughout changes in muscle morphology and neuromuscular function. Notwithstanding, besides the conflicting results, EMG amplitudes obtained during motion activities demonstrate that the neuromuscular strategy and control may be dependent on the treatment received [33]. Mathematical and computational modeling can help investigate the characteristics of EMG signals and test their accuracy and validity. Mathematical modeling allows the estimation of parameters that are not directly accessible for measurements, for example, related to the description of the spatial and temporal recruitment of motor units [34]. Moreover, it can help in developing tools to measure the force developed by a muscle [35].

The objective here is to reproduce the behavior of muscle contraction using a coupled model of force generation and the action potential of the cell membrane, associated with Ca^{2+} regulation, inserting the latency period observed between the action potential in the membrane and force generation in the motor unit.

2 Materials and methods

2.1 Calcium dynamics and muscle contraction models

The mathematical model of calcium dynamics and muscle contraction was based on the work in [36] that appears in the work in [37] and [38], which uses simple mass action kinetics to describe calcium dynamics in the muscle. The model is shown in Figure 2. It describes the relationship between concentrations of free calcium ions $[c]$, unbound SR calcium binding $[s]$, unbound contractile filaments (CFs) calcium binding $[f]$, calcium-bound SR sites $[cs]$, and calcium-bound CF sites $[cf]$.

The rates at which reactants act are represented by parameters k_i. The rates k_1 and k_2 operate similar to a switch, dependent on the

value of the action potential of muscle V_m, as shown by the following equations:

$$k_1\left(V_m\left(t-T\right)\right) = \begin{cases} k_1, & \text{if } V_m\left(t-T\right) > V_{min}, \\ 0, & \text{otherwise} \end{cases} \quad (1)$$

$$k_2\left(V_m\left(t-T\right)\right) = \begin{cases} k_2, & \text{if } V_m\left(t-T\right) < V_{min}, \\ 0, & \text{otherwise} \end{cases} \quad (2)$$

where V_m is the action potential in the membrane, V_{min} is its minimum value to activate the contraction process, and T is the latency period (in ms) between the action potential in the membrane and the onset of contraction. The inclusion of delay was implemented by a delay-differential equation (DDE), as evaluated in [39], which achieved dynamics similar to the original FitzHugh–Nagumo and Hodgkin–Huxley models using a single DDE formulation in each case.

When a muscle is activated, k_1 represents the rate constant for the release of calcium from the SR and $k_2 = 0$. When the muscle is not activated, $k_1 = 0$ and k_2 represent the rate constant for the binding of calcium to the SR. Likewise, the rate of binding of calcium-bound CF sites is proportional to the concentration of both free calcium ions and unbound calcium-binding sites with rate constant k_3. The reversible process occurs with rate constant k_4, and it is proportional to the concentration of both bound and unbound CF sites. In [38], it was explained that it was necessary to introduce some cooperativity in the release of calcium so that the relaxation process does not begin abruptly. Although different from the relationship of k_1 and k_2, k_3 and k_4 can both be non-zero at the same time. The differential equations of calcium dynamics are as follows:

$$\frac{d[c]}{dt} = k_1[cs] - k_2[c][s] - k_3[c][f] + k_4[cf][f], \quad (3)$$

$$\frac{d[cs]}{dt} = -k_1[cs] + k_2[c][s], \quad (4)$$

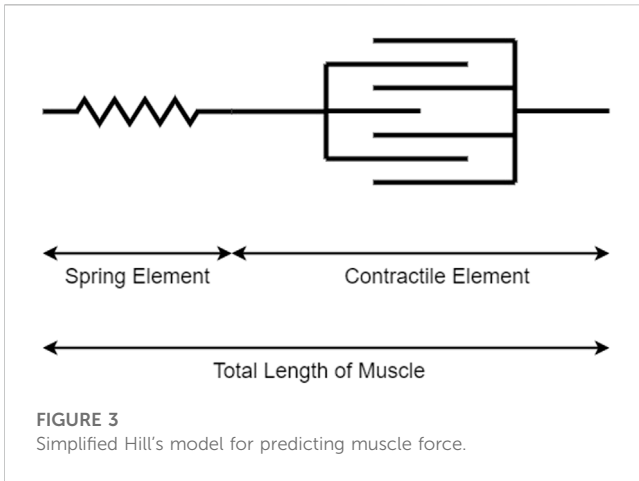$$\frac{d[s]}{dt} = k_1[cs] - k_2[c][s], \quad (5)$$

FIGURE 3
Simplified Hill's model for predicting muscle force.

TABLE 1 Input parameters for the action potential model.

Parameter	Value	Citation
k_1 (activated)	9.6 s^{-1}	[37]
k_2 (activated)	5.9 s^{-1}	[37]
k_3	65 s^{-1}	[37]
k_4	45 s^{-1}	[37]
k_5	100 s^{-1}	[37]
C	15	-
S	15	-
F	15	-
L	2.7 mm	[37]
μ_0	1	[38]
μ_1	23	[38]
λ_2	−20	[38]
l_{c0}	2.6 mm	[37]
α_{max}	1.8	[37]
α_p	1.33 s/mm	[37]
α_m	0.4 s/mm	[37]
V_{min}	−20 mV	-
T	10 ms	[2]

$$\frac{d[cf]}{dt} = k_3[c][f] - k_4[cf][f], \qquad (6)$$

$$\frac{d[f]}{dt} = -k_3[c][f] + k_4[cf][f]. \qquad (7)$$

It is assumed the total number of calcium ions (C), SR-binding sites (S), and filament-binding sites (F) remains constant, following mass conservation laws:

$$[c] + [cf] + [cs] = C, \qquad (8)$$

$$[s] + [cs] = S, \qquad (9)$$

$$[f] + [cf] = F. \qquad (10)$$

Combining the differential equations from mass action kinetics and mass conservation laws yields

$$\frac{d[c]}{dt} = k_1(C - [c] - [cf]) - k_2[c](S - C + [c] + [cf]) - k_3[c](F - [cf]) + k_4[cf](F - [cf]) \qquad (11)$$

$$\frac{d[cf]}{dt} = k_3[c](F - [cf]) - k_4[cf](F - [cf]). \qquad (12)$$

Accordingly to the work in [3], there are three general classes of models for predicting muscle force: biochemical models, constitutive models, or Hill's models. In [36], Hill's model based on the work in [40] was used, which describes the muscle as a contractile element in series with a linearly spring element, as shown in Figure 3. The model says that the total length of muscle corresponds to the length of the contractile element l_c plus the length of the linearly spring element l_s:

$$L = l_c + l_s. \qquad (13)$$

According to Hooke's law, the total force in a linearly elastic body is proportional to the final length of that body minus the initial length:

$$P_s = \mu_s(l_s - l_{s_0}), \qquad (14)$$

where P_s is the applied force, l_s is the final length, l_{s_0} is the initial length, and the proportionality constant μ_s is Young's modulus, or stiffness constant. In Hill's model, that stiffness varies when muscle exerts force from total relaxation.

$$\mu_s = \mu_0 + \mu_1[cf]. \qquad (15)$$

Combining Eq. 13 with Eq. 14 and isolating l_c yield

$$l_c = L - \frac{P_s}{\mu_s} + l_{s_0}. \qquad (16)$$

Taking the time derivative of Eq. 16 yields

$$v_c = V(t) - \frac{dP_s}{dt}\frac{1}{\mu_s} + \frac{\mu_1 P_s}{\mu_s^2}\frac{d[cf]}{dt}, \qquad (17)$$

where v_c and $V(t)$ are the time derivatives of l_c and L, respectively.

Assuming that the muscle performs an isometric contraction, its total length $L(t)$ is constant, and time derivative $V(t)$ is null.

As assumed in [36], the applied force on the contractile element (P_c) is proportional to independent multiplicative factors of its length (l_c) and velocity (v_c):

$$P_c = P_0\lambda(l_c)\alpha(v_c)[cf]. \qquad (18)$$

Furthermore, dividing Eq. 18 by P_0 provides a non-dimensional value for P_c, as was carried out in [38].

$$P_c = \lambda(l_c)\alpha(v_c)[cf]. \qquad (19)$$

The functions $\lambda(l_c)$ and $\alpha(v_c)$ were measured in [36], which provided a linear function for α and a quadratic function for λ as follows:

TABLE 2 Initial conditions for each variable.

Variable	Value	Citation
c	0	-
cf	0	-
P	$0\ N$	-
V_m	$-70\ mV$	[45]
m	0.05	[42]
n	0.3	[42]
h	0.6	[42]

$$\alpha(v_c) = 1 + \begin{cases} \alpha_m v_c & \text{if } v_c < 0 \\ \alpha_p v_c & \text{if } v_c \geq 0 \end{cases},\qquad (20)$$

$$\lambda(l_c) = 1 + \lambda_2(l_c - l_{c0})^2. \qquad (21)$$

These functions are restricted such that $0 \leq \alpha(v_c) \leq \alpha_{max}$ and $0 \leq \lambda(l_c) \leq 1$. According to [3], when muscle performs concentric contractions, i.e., the shortening of fiber muscle occurs, the relationship between force and velocity is nearly hyperbolic and relatively lower than when it performs eccentric contractions (lengthening of fiber muscle). This fact reflects $\alpha_p > \alpha_m > 0$.

In a steady state, P_s and P_c must be equal. So, the transfer of force from the contractile element to the spring element was modeled by simple linear kinetics:

$$\frac{dP_s}{dt} = k_5(P_c - P_s), \qquad (22)$$

where k_5 is a selected parameter to approximate P_c to P_s.

To prevent instability, Eq. 17 was combined with Eq. 19 and Eq. 20:

$$P_c = \lambda\left(1 - \frac{dP_s}{dt}\frac{\alpha}{\mu_s} + \frac{\alpha\mu_1 P_s}{\mu_s{}^2}\frac{d[cf]}{dt}\right)[cf], \qquad (23)$$

$$\alpha(v_c) = \begin{cases} \alpha_m & \text{if } v_c < 0 \\ \alpha_p & \text{otherwise.} \end{cases} \qquad (24)$$

Finally, Eq. 23 was combined with Eq. 22, and isolating the time derivative $\frac{dP}{dt}$, the model of muscle force was obtained:

$$\frac{dP_s}{dt} = \frac{\lambda[cf]\left(1 + \frac{\alpha\mu_1}{\mu_s{}^2}\frac{d[cf]}{dt}\right) - P_s}{\frac{1}{k_5} + \frac{\lambda\alpha[cf]}{\mu_s}}. \qquad (25)$$

The constants used for calcium dynamics and muscle contraction models are given in Table 1. The value of V_{min} was arbitrarily chosen by the authors to represent a minimum threshold that must be reached for the contraction to actually occur. In the future, it is possible to compare it with real data to adjust this parameter. Although the model used here shares its foundation with the model in [36], it introduces a previously unaccounted latency period (T). As explained in [2], this latency period represents the delay between the arrival of the action potential and the release of Ca^{+2} in the muscle cell, typically averaging between 3 and 10 ms. Thus, the value of T was derived from the established literature.
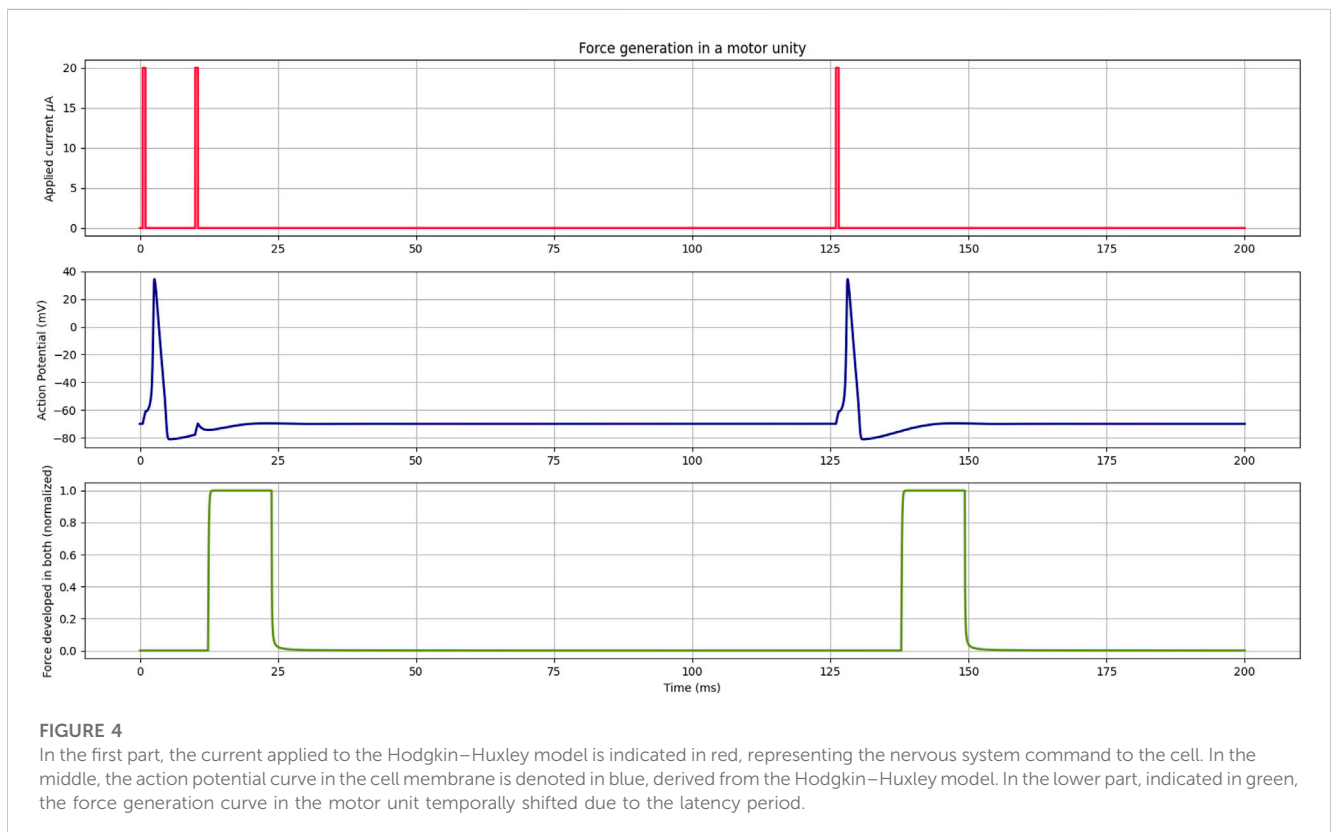

FIGURE 4
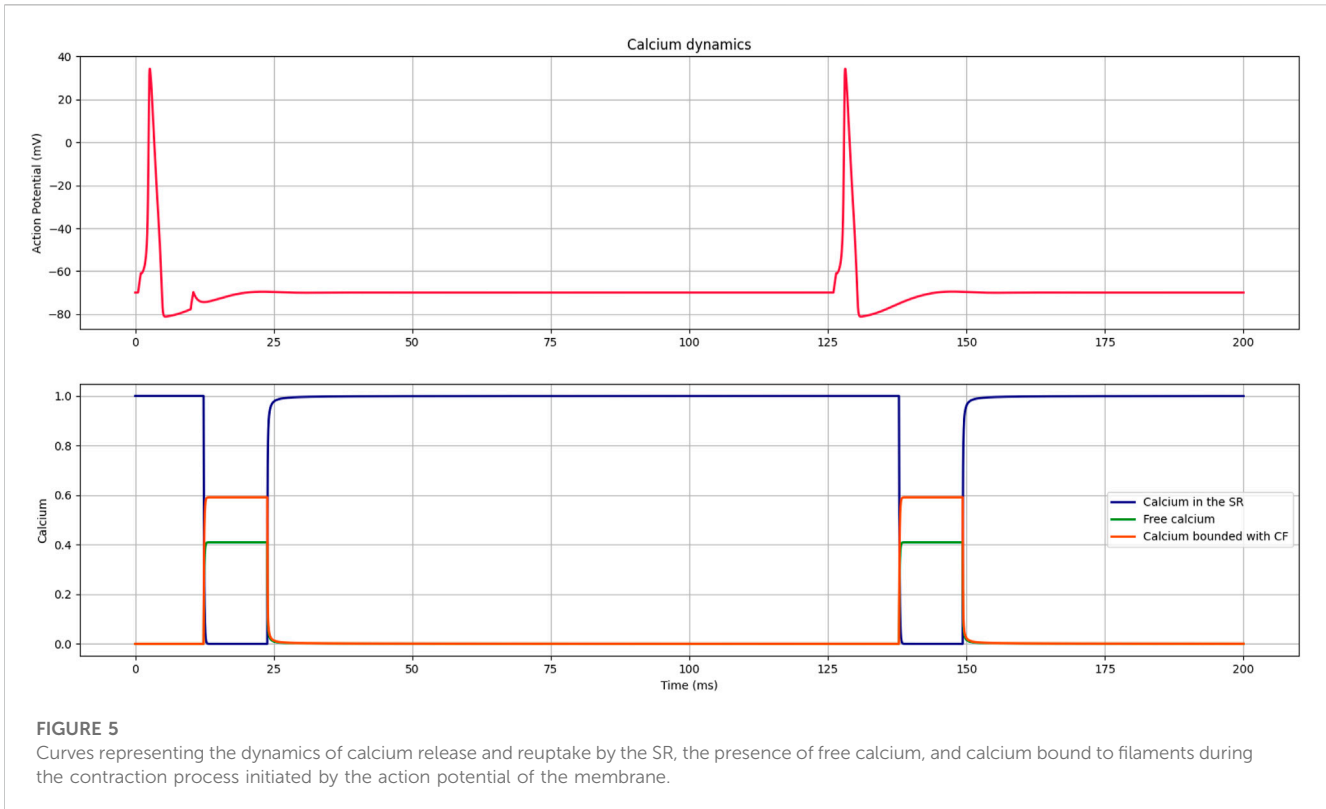In the first part, the current applied to the Hodgkin−Huxley model is indicated in red, representing the nervous system command to the cell. In the middle, the action potential curve in the cell membrane is denoted in blue, derived from the Hodgkin−Huxley model. In the lower part, indicated in green, the force generation curve in the motor unit temporally shifted due to the latency period.

FIGURE 5
Curves representing the dynamics of calcium release and reuptake by the SR, the presence of free calcium, and calcium bound to filaments during
the contraction process initiated by the action potential of the membrane.

2.2 Action potential model

The contraction in a motor unit begins with an action potential
reaching the motor end plate and neurotransmitters being released in
the synaptic cleft. This causes Ca^{2+} to be released into the cytoplasm of
the muscle cell. In [36] and [38], a high-frequency sequence of
individual stimuli, called tetanic stimulus [38], was used, while in
[37], stimuli were created based on square and exponential
functions to represent tetanic stimulus and individual electric impulse.

Here, the stimulus in the cell membrane that activates the
calcium dynamic is the action potential from the model
described by [41], explained in the Appendices. The
Hodgkin–Huxley model was chosen due to its accurate
representation of the action potential, as well as being a simpler
model (with only four differential equations) compared to more
recent ones. Considering the potential for simulating multiple motor
units, larger models become computationally expensive. The
FitzHugh–Nagumo model was also assessed for having only two
equations; however, its representation is less faithful than that of the
Hodgkin–Huxley model [42]. Moreover, many recent studies were
based on the formalism of the Hodgkin–Huxley model, while many
others employ an even simpler formulation based on a transfer
function, as indicated in [43]. As shown in [37], the stimulus is
responsible for changing the rates k_1 and k_2.

2.3 Numerical method

The numerical method applied to solve Eqs 11, 12, 25, A1–A–A4
was Euler's method, or forward Euler, which replaces the derivative
term by the approximation presented in the following equation [44]:

$$\frac{dU}{dt} = \frac{U^{i+1} - U^i}{k},\qquad(26)$$

where U is the variable of interest, k is the discretization time step,
and i indicates which time step the variable U is in. This way, it was
possible to approximate variable U in time $i + 1$, starting from the
time $t = 0$, in which the state of the variables is known. So, starting
with a relaxed muscle, the membrane is at rest (without an action
potential), all calcium is in the SR, and, consequently, there is no
force developed. Thus, Table 2 shows the initial conditions used in
this paper. The conditions were chosen based on the idea that there
is no free calcium or calcium bound to filaments initially, and the cell
membrane is at rest. The value of V_m was chosen according to the
work in [45] and the variables m, n, and h according to the work
in [42].

Compared to the backward Euler and Crank–Nicolson
model, it is faster, which is great for optimizing time
simulations. The system of equations was solved using an
algorithm implemented in Python with $k = 0.001$, and their
exploitation about how it was implemented is presented in the
following equations.

The ODE refers to free calcium ions:

$$[c^{i+1}] = [c^i] + k[k_1(C - [c^i] - [cf^i]) - k_2[c^i](S - C + [c^i] + [cf^i])$$

$$- k_3[c^i](F - [cf^i])].\qquad(27)$$

The ODE refers to calcium-bound CF sites:

$$[cf^{i+1}] = [cf^i] + k[k_3[cf^i](F - [cf^i]) - k_4[cf^i](F - [cf^i])].$$
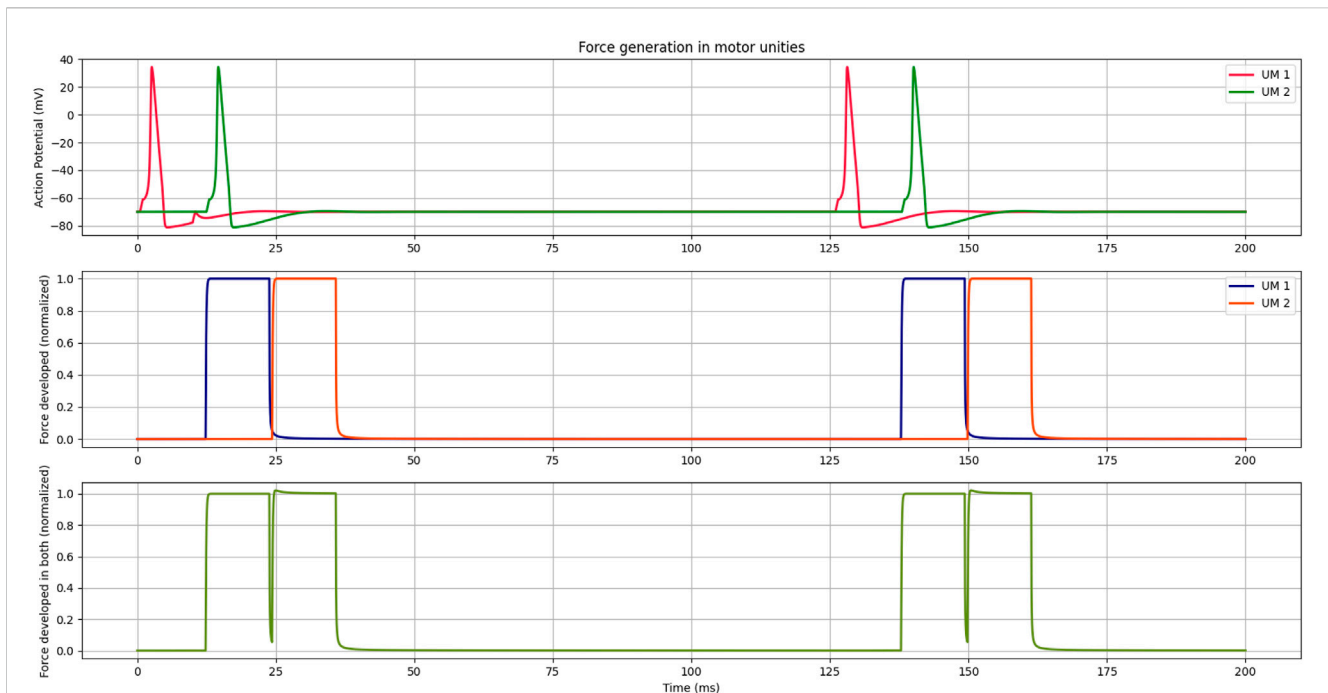
$$(28)$$

FIGURE 6
The first part shows the action potential curves of two different motor units being stimulated. The second part shows the forces developed in both. The third part shows the combined force of both, representing how it would be in a muscle.

The ODE refers to the force developed by the muscle:

$$P_s^{i+1} = P_s^i + k \left[\frac{\lambda [cf^i]\left(1 + \frac{\alpha\mu_1 P_s^i}{\mu_s^i} \frac{d[cf^i]}{dt}\right) - P_s^i}{\frac{1}{k_5} + \frac{\lambda\alpha[cf^i]}{\mu_s}} \right]. \tag{29}$$

The ODE refers to an action potential in the membrane:

$$V_m^{i+1} = V_m^i + k \left(\frac{I_{app}^i - I_{Na}^i - I_K^i - I_L^i}{C_m} \right), \tag{30}$$

where

$$I_{Na}^{i+1} = \bar{g}_{Na} m^i h^i \left(V_m^i - V_{Na} \right), \tag{31}$$

$$I_K^{i+1} = \bar{g}_K n^4 h^i \left(V_m^i - V_K \right), \tag{32}$$

$$I_L^{i+1} = \bar{g}_L \left(V_m^i - V_L \right). \tag{33}$$

The ODE refers to auxiliary variables:

$$n^{i+1} = n^i + k \left[\alpha_n \left(1 - n^i \right) - \beta_n n^i \right], \tag{34}$$

$$m^{i+1} = m^i + k \left[\alpha_m \left(1 - m^i \right) - \beta_m m^i \right], \tag{35}$$

$$h^{i+1} = h^i + k \left[\alpha_h \left(1 - h^i \right) - \beta_h h^i \right]. \tag{36}$$

3 Results

The contraction process begins with a command from the nervous system, represented here by applied current I_{app}, in the first part of Figure 4. When the stimulus is large enough to generate the action potential, calcium is released, leading to the contraction of the motor unit.

As shown in blue in Figure 4, where current I_{app} has two consecutive stimuli before 25 ms, the Hodgkin–Huxley model has a refractory period that prevents another action potential from occurring while one was already being developed. Consequently, there was no force generation due to this second current stimulus. However, stimuli applied after the refractory period generate an action potential and, after the latency period, force in the motor unit once again. Since it was set that calcium would be released starting at a value of −20 mV, the 10-ms latency period was observed from this point. The selection of different values for V_{min} would cause the contraction to start earlier or later, depending on the value. Here, the value was arbitrary to represent the threshold of the muscle cell.

Figure 5 illustrates the dynamic initiated by an action potential; first, all the calcium ions are stored in the SR, and once the potential is generated, they are released and bind to the filaments. After some time, the process is reversed, and all the calcium returns to SR.

Finally, Figure 6 shows that a muscle stimulus was simulated using two motor units to verify the total tension generated in the muscle. It can be considered that when a high load is demanded in major time, lots of motor units are stimulated, resulting in a higher or longer-lasting tension developed in the muscle.

4 Discussion

A simulation coupling the Hodgkin–Huxley action potential model to the models demonstrated in [36], [38], and [37] was presented, adding the latency period between the stimulus and muscle contraction to approximate the model to the real behavior of the muscle. Although the Hodgkin–Huxley model is relatively old, it remains a significant global reference and is integrated into numerous research studies across the vast field of

the electrophysiology community. Despite its use, certain biological processes such as the activation of ion channels in the SR by the entry of calcium for subsequent release were simplified by delay T because that model does not include those processes.

The control over the rates was also different from that shown in [37] because here, the Hodgkin–Huxley model was used to determine the nervous stimulus associated with the release and resorption of calcium by the SR. Therefore, the Hodgkin–Huxley model introduced the dynamics of the sodium and potassium ions as electrical current components, along with the calcium dynamics in the model, which is an important component of the skeletal muscle contraction behavior [46].

The focus of this study was on muscle behavior, simulating reduced-size motor units. Nevertheless, it paves the way to associate and distinguish the influence of electrical stimuli and calcium ion dynamics on healthy muscle contraction. The question remains as to whether alterations in muscle contraction dynamics during certain illnesses are attributed to changes in electrical conduction or disruptions in calcium dynamics. Hence, future efforts should involve comparing results obtained from full-sized scenarios with a higher number of motor units, as well as incorporating data collected from both healthy individuals and those who have undergone cancer treatment.

Data availability statement

The original contributions presented in the study are included in the article/Supplementary Material; further inquiries can be directed to the corresponding author.

Author contributions

NK, AG, GL, RW, SV, and FB: writing–original draft. AG and GL: Software.

Conflict of interest

The authors declare that the research was conducted in the absence of any commercial or financial relationships that could be construed as a potential conflict of interest.

Publisher's note

All claims expressed in this article are solely those of the authors and do not necessarily represent those of their affiliated organizations, or those of the publisher, the editors, and the reviewers. Any product that may be evaluated in this article, or claim that may be made by its manufacturer, is not guaranteed or endorsed by the publisher.

References

1. Li F, Periasamy M. Skeletal muscle inefficiency protects against obesity. *Nat Metab* (2019) 1:849–50. doi:10.1038/s42255-019-0116-x

2. Ethier CR, Simmons CA. *Introductory biomechanics: from cells to organisms.* Cambridge: Cambridge University Press (2007).

3. Peterson DR, Bronzino JD. *Biomechanics: principles and applications.* Florida, United States: CRC Press (2007).

4. Lynch CL. *Closed-loop control of electrically stimulated skeletal muscle contractions.* Toronto, Canada: University of Toronto (2011).

5. Farina D, Fosci M, Merletti R. Motor unit recruitment strategies investigated by surface emg variables. *J Appl Physiol* (2002) 92:235–47. doi:10.1152/jappl.2002.92.1.235

6. Heckman C, Enoka RM. Motor unit. *Compr Physiol* (2012) 2629–82. doi:10.1002/cphy.c100087

7. Baker LL, Parker K. Neuromuscular electrical stimulation of the muscles surrounding the shoulder. *Phys Ther* (1986) 66:1930–7. doi:10.1093/ptj/66.12.1930

8. Chaparro-Cárdenas SL, Castillo-Castañeda E, Lozano-Guzmán AA, Zequera M, Gallegos-Torres RM, Ramirez-Bautista JA. Characterization of muscle fatigue in the lower limb by semg and angular position using the wfd protocol. *Biocybernetics Biomed Eng* (2021) 41:933–43. doi:10.1016/j.bbe.2021.06.003

9. Cavalcanti Garcia MA, Magalhães J, Imbiriba L. Temporal behavior of motor units action potential velocity under muscle fatigue conditions. *Revista Brasileira de Medicina do Esporte* (2004) 10:299–303. doi:10.1590/S1517-86922004000400007

10. Moretti A, Iolascon G. Sclerostin: clinical insights in muscle–bone crosstalk. *J Int Med Res* (2023) 51. doi:10.1177/03000605231193293

11. Ferrucci L, Baroni M, Ranchelli A, Lauretani F, Maggio M, Mecocci P, et al. Interaction between bone and muscle in older persons with mobility limitations. *Curr Pharm Des* (2014) 20:3178–97. doi:10.2174/13816128113196660690

12. Stožer A, Vodopivc P, Križančić Bombek L. Pathophysiology of exercise-induced muscle damage and its structural, functional, metabolic, and clinical consequences. *Physiol Res* (2020) 565–98. doi:10.33549/physiolres.934371

13. Allen DG. Skeletal muscle function: role of ionic changes in fatigue, damage and disease. *Clin Exp Pharmacol Physiol* (2004) 31:485–93. doi:10.1111/j.1440-1681.2004.04032.x

14. Aichi M, Hasegawa S, Kurita Y, Shinoda S, Kato S, Mizushima T, et al. Low skeletal muscle mass predicts poor prognosis for patients with stage iii cervical cancer on concurrent chemoradiotherapy. *Nutrition* (2023) 109:111966. doi:10.1016/j.nut.2022.111966

15. Abe A, Yuasa M, Imai Y, Kagawa T, Mineda A, Nishimura M, et al. Extreme leanness, lower skeletal muscle quality, and loss of muscle mass during treatment are predictors of poor prognosis in cervical cancer treated with concurrent chemoradiation therapy. *Int J Clin Oncol* (2022) 27:983–91. doi:10.1007/s10147-022-02140-w

16. Ji C, Liu S, Wang C, Chen J, Wang J, Zhang X, et al. Relationship between visceral obesity and prognosis in patients with stage ivb cervical cancer receiving radiotherapy and chemotherapy. *Cancer Pathogenesis Ther* (2023). doi:10.1016/j.cpt.2023.09.002

17. Deng Y, Zhao L, Huang X, Zeng Y, Xiong Z, Zuo M. Contribution of skeletal muscle to cancer immunotherapy: a focus on muscle function, inflammation, and microbiota. *Nutrition* (2023) 105:111829. doi:10.1016/j.nut.2022.111829

18. Schneider CM, Hsieh CC, Sprod LK, Carter SD, Hayward R. Cancer treatment-induced alterations in muscular fitness and quality of life: the role of exercise training. *Ann Oncol* (2007) 18:1957–62. doi:10.1093/annonc/mdm364

19. Kirchheiner K, Pötter R, Tanderup K, Lindegaard JC, Haie-Meder C, Petrič P, et al. Health-related quality of life in locally advanced cervical cancer patients after definitive chemoradiation therapy including image guided adaptive brachytherapy: an analysis from the embrace study. *Int J Radiat Oncology*Biology*Physics* (2016) 94:1088–98. doi:10.1016/j.ijrobp.2015.12.363

20. Buffart LM, Sweegers MG, de Ruijter CJ, Konings IR, Verheul HMW, van Zweeden AA, et al. Muscle contractile properties of cancer patients receiving chemotherapy: assessment of feasibility and exercise effects. *Scand J Med Sci Sports* (2020) 30:1918–29. doi:10.1111/sms.13758

21. Visovsky C. Muscle strength, body composition, and physical activity in women receiving chemotherapy for breast cancer. *Integr Cancer Ther* (2006) 5:183–91. doi:10.1177/1534735406291962

22. Tofthagen C, Visovsky CM, Hopgood R. Chemotherapy-induced peripheral neuropathy. *Clin J Oncol Nurs* (2013) 17:138–44. doi:10.1188/13.CJON.138-144

23. Avelino SOM, Neves RM, Sobral-Silva LA, Tango RN, Federico CA, Vegian MRC, et al. Evaluation of the effects of radiation therapy on muscle contractibility and skin healing: an experimental study of the cancer treatment implications. *Life (Basel)* (2023) 13. doi:10.3390/life13091838

24. Santos JCM, Jr. Radioterapia: lesões inflamatórias e funcionais de órgãos pélvicos. *Revista Brasileira de Coloproctologia* (2006) 26:348–55. doi:10.1590/S0101-98802006000300019

25. Bernard S, Moffet H, Plante M, Ouellet MP, Leblond J, Dumoulin C. Pelvic-floor properties in women reporting urinary incontinence after surgery and radiotherapy for endometrial cancer. *Phys Ther* (2017) 97:438–48. doi:10.1093/ptj/pzx012

26. Miguel TP, Laurienzo CE, Faria EF, Sarri AJ, Castro IQ, Affonso RJ, et al. Chemoradiation for cervical cancer treatment portends high risk of pelvic floor dysfunction. *PLoS ONE* (2020) 15:1–12. doi:10.1371/journal.pone.0234389

27. Maduro J, Pras E, Willemse P, de Vries E. Acute and long-term toxicity following radiotherapy alone or in combination with chemotherapy for locally advanced cervical cancer. *Cancer Treat Rev* (2003) 29:471–88. doi:10.1016/S0305-7372(03)00117-8

28. Spampinato S, Tanderup K, Lindegaard JC, Schmid MP, Sturdza A, Segedin B, et al. Association of persistent morbidity after radiotherapy with quality of life in locally advanced cervical cancer survivors. *Radiother Oncol* (2023) 181:109501. doi:10.1016/j.radonc.2023.109501

29. Lind H, Waldenström AC, Dunberger G, al Abany M, Alevronta E, Johansson KA, et al. Late symptoms in long-term gynaecological cancer survivors after radiation therapy: a population-based cohort study. *Br J Cancer* (2011) 105:737–45. doi:10.1038/bjc.2011.315

30. Gadducci A, Simonetti E, Mezzapesa F, Cosio S, Miccoli M, Frey J, et al. Computed tomography-assessed skeletal muscle index and skeletal muscle radiation attenuation in patients with ovarian cancer treated with primary surgery followed by platinum-based chemotherapy: a single-center Italian study. *Anticancer Res* (2022) 42:947–54. doi:10.21873/anticanres.15554

31. Polen-De C, Fadadu P, Weaver AL, Moynagh M, Takahashi N, Jatoi A, et al. Quality is more important than quantity: pre-operative sarcopenia is associated with poor survival in advanced ovarian cancer. *Int J Gynecol Cancer* (2022) 32. doi:10.1136/ijgc-2022-003387

32. Klotz T, Gizzi L, Yavuz UŞ, Röhrle O. Modelling the electrical activity of skeletal muscle tissue using a multi-domain approach. *Biomech Model Mechanobiol* (2020) 19: 335–49. doi:10.1007/s10237-019-01214-5

33. Leonardis JM, Lulic-Kuryllo T, Lipps DB. The impact of local therapies for breast cancer on shoulder muscle health and function. *Crit Rev Oncology/Hematology* (2022): 103759. doi:10.1016/j.critrevonc.2022.103759

34. Mesin L. Volume conductor models in surface electromyography: computational techniques. *Comput Biol Med* (2013) 43:942–52. doi:10.1016/j.compbiomed.2013.02.002

35. Staudenmann D, Kingma I, Daffertshofer A, Stegeman DF, vanDieen JH. Improving EMG-based muscle force estimation by using a high-density EMG grid and principal component analysis. *IEEE Trans Biomed Eng* (2006) 53:712–9. doi:10.1109/TBME.2006.870246

36. McMillen T, Williams T, Holmes P. Nonlinear muscles, passive viscoelasticity and body taper conspire to create neuromechanical phase lags in anguilliform swimmers. *PLOS Comput Biol* (2008) 4:1–16. doi:10.1371/journal.pcbi.1000157

37. Meredith T. *A mathematical model of the neuromuscular junction and muscle force generation in the pathological condition myasthenia gravis*. Seattle: Semantic Scholar (2018). *Art* **52036412**.

38. Williams TL. A new model for force generation by skeletal muscle, incorporating work-dependent deactivation. *J Exp Biol* (2010) 213:643–50. doi:10.1242/jeb.037598

39. Rameh RB, Cherry EM, dos Santos RW. Single-variable delay-differential equation approximations of the fitzhugh-nagumo and hodgkin-huxley models. *Commun Nonlinear Sci Numer Simulation* (2020) 82:105066. doi:10.1016/j.cnsns.2019.105066

40. Hill AV. The heat of shortening and the dynamic constants of muscle. *Proc R Soc Lond Ser B-Biological Sci* (1938) 126:136–95. doi:10.1098/rspb.1938.0050

41. Hodgkin AL, Huxley AF. A quantitative description of membrane current and its application to conduction and excitation in nerve. *J Physiol* (1952) 117:500. doi:10.1113/jphysiol.1952.sp004764

42. Keener J, Sneyd J. *Mathematical physiology: II: systems physiology*. Cham: Springer (2009).

43. Haggie L, Schmid L, Röhrle O, Besier T, McMorland A, Saini H. Linking cortex and contraction—integrating models along the corticomuscular pathway. *Front Physiol* (2023) 14:1095260. doi:10.3389/fphys.2023.1095260

44. LeVeque RJ. *Finite difference methods for ordinary and partial differential equations: steady-state and time-dependent problems*. Philadelphia, Pennsylvania, USA. SIAM (2007).

45. Hopkins PM. Skeletal muscle physiology. *Continuing Edu Anaesth Crit Care Pain* (2006) 6:1–6. doi:10.1093/bjaceaccp/mki062

46. Sweeney HL, Hammers DW. Muscle contraction. *Cold Spring Harbor Perspect Biol* (2018) 10. doi:10.1101/cshperspect.a023200

47. Boylestad RL. *Introductory circuit analysis*. Hoboken, New Jersey: Prentice Hall Press (2010).

Appendix A

Hodgkin–Huxley model

The conductance-based model describes the potential using the currents passing through the membrane. Figure A1 shows the electrical circuit that represents this phenomenon, which presents a capacitor representing the membrane (C_m), resistors and sources to represent the ion channels (potassium V_K, sodium V_{Na}, and others V_L), and an applied current to indicate the stimulus from the nervous system (I_{app}).

Kirchhoff's first law [47] was applied to the circuit shown in Figure A1 to determinate Eq. A1, which describes the action potential in the membrane, where $\bar{g}_{Na}$, $\bar{g}_K$, and $\bar{g}_L$ are the conductance of the channels of sodium, potassium, and other ions, V_{Na}, V_K, and V_L are the potential differences of these channels, and C_m is the membrane conductance. Eqs A2–A4 represent the auxiliary variables n, m, and h, as described in [41]. These equations use alpha (α) and beta (β) functions, as also described in [41], which are given in Eqs A5–A10. All constants used for the membrane action potential model are given in Table A1.

$$\frac{d[V_m]}{dt} = \frac{1}{C_m}\left[I_{app} - \bar{g}_k n^4 (V_m - V_k) - \bar{g}_{Na} m^3 h (V_m - V_{Na}) - \bar{g}_l (V_m - V_l)\right], \tag{A1}$$

$$\frac{dn}{dt} = \alpha_n (1 - n) - \beta_n n, \tag{A2}$$

$$\frac{dm}{dt} = \alpha_m (1 - m) - \beta_m m, \tag{A3}$$

$$\frac{dh}{dt} = \alpha_h (1 - h) - \beta_h h, \tag{A4}$$

$$\alpha_n = \frac{0.01 (10 - V_m)}{e^{\frac{10 - V_m}{10}} - 1}, \tag{A5}$$

$$\beta_n = 0.125 e^{\frac{-V_m}{80}}, \tag{A6}$$

$$\alpha_m = \frac{0.1 (25 - V_m)}{e^{\frac{25 - V_m}{10}} - 1}, \tag{A7}$$

$$\beta_m = 4 e^{\frac{-V_m}{18}}, \tag{A8}$$

$$\alpha_h = 0.07 e^{\frac{-V_m}{20}}, \tag{A9}$$

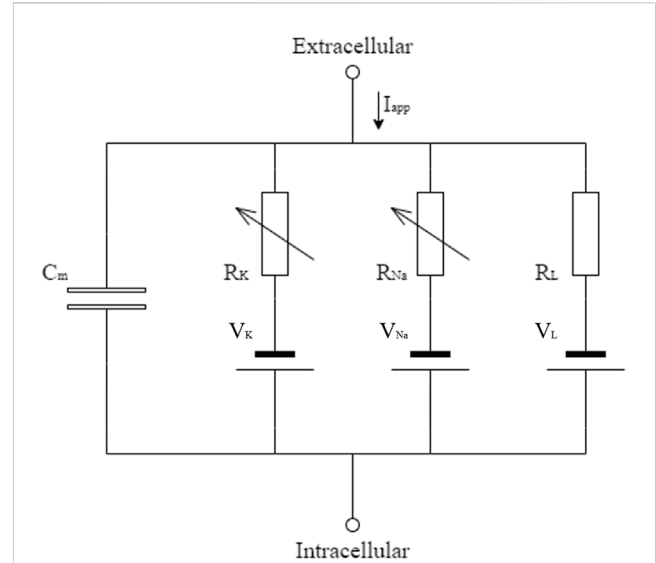$$\beta_h = \frac{1}{e^{\frac{-V_m}{10}} + 1}. \tag{A10}$$

FIGURE A1
Electric circuit representing the cellular membrane, as described in [41].

TABLE A1 Input parameters for the action potential model.

Parameter	Value	Citation
C_m	$1\ \mu F/cm^2$	[42]
$\bar{g}_{Na}$	$120\ mS/cm^2$	[42]
$\bar{g}_K$	$36\ mS/cm^2$	[42]
$\bar{g}_L$	$0.3\ mS/cm^2$	[42]
V_{Na}	$115\ mV$	[42]
V_K	$-12\ mV$	[42]
V_L	$10.6\ mV$	[42]